Thermally stable, highly efficient, ultraflexible organic photovoltaics

Xiaomin Xu[a,1,2], Kenjiro Fukuda[a,b,c,1,3], Akchheta Karki[d], Sungjun Park[a], Hiroki Kimura[a,e], Hiroaki Jinno[a,f], Nobuhiro Watanabe[g], Shuhei Yamamoto[g], Satoru Shimomura[g], Daisuke Kitazawa[g], Tomoyuki Yokota[f], Shinjiro Umezu[e], Thuc-Quyen Nguyen[d], and Takao Someya[a,b,f,3]

[a]Center for Emergent Matter Science, RIKEN, Wako, 351-0198 Saitama, Japan; [b]Thin-Film Device Laboratory, RIKEN, Wako, 351-0198 Saitama, Japan; [c]Japan Science and Technology Agency, Precursory Research for Embryonic Science and Technology, Kawaguchi, 332-0012 Saitama, Japan; [d]Center for Polymers and Organic Solids, University of California, Santa Barbara, CA 93106; [e]Department of Modern Mechanical Engineering, Waseda University, Shinjuku, 169-8555 Tokyo, Japan; [f]Electrical and Electronic Engineering and Information Systems, The University of Tokyo, 113-8656 Tokyo, Japan; and [g]Advanced Materials Research Laboratories, Toray Industries, Inc., Otsu, 520-0842 Shiga, Japan

Edited by Stephen R. Forrest, University of Michigan, Ann Arbor, MI, and approved March 19, 2018 (received for review January 21, 2018)

Flexible photovoltaics with extreme mechanical compliance present appealing possibilities to power Internet of Things (IoT) sensors and wearable electronic devices. Although improvement in thermal stability is essential, simultaneous achievement of high power conversion efficiency (PCE) and thermal stability in flexible organic photovoltaics (OPVs) remains challenging due to the difficulties in maintaining an optimal microstructure of the active layer under thermal stress. The insufficient thermal capability of a plastic substrate and the environmental influences cannot be fully expelled by ultrathin barrier coatings. Here, we have successfully fabricated ultraflexible OPVs with initial efficiencies of up to 10% that can endure temperatures of over 100 °C, maintaining 80% of the initial efficiency under accelerated testing conditions for over 500 hours in air. Particularly, we introduce a low-bandgap poly(benzodithiophene-cothieno[3,4-b]thiophene) (PBDTTT) donor polymer that forms a sturdy microstructure when blended with a fullerene acceptor. We demonstrate a feasible way to adhere ultraflexible OPVs onto textiles through a hot-melt process without causing severe performance degradation.

organic photovoltaics | thermal stability | power conversional efficiency | ultraflexibility

Power sources that are flexible enough to be attached onto curved and rough surfaces are one of the most promising solutions to supplying electrical power directly to Internet of Things sensors, wearable sensors, and electronic devices. As one of the thinnest, lightest, and most flexible photovoltaic technologies, organic photovoltaics (OPVs) are promising for extensive integration in various shapes and sizes, thus extending power sources from space-intensive to the prevailing wearable form of electronics.

The power conversion efficiency (PCE) of OPVs improved from 1 to 10% (1–4), which is considered a representative efficiency for widespread applications. A latest rational design of a single-junction binary blend brings the record value up to 13.1% (5). Such a high performance has been demonstrated using rigid glass substrates. After considerable progress was made on the development of highly efficient OPVs on rigid substrates, an outlook was presented on driving this emerging technology with combined mechanical conformability. Based on the success of material design, the optimization of flexible electrodes, and strategies for enhanced light–matter interactions, flexible OPVs with millimeter-scale bending radii have been developed rapidly with the PCEs increasing from below 3% (6) up to 9.4% (7). Further reducing the total thickness to several micrometers imparts extreme mechanical compliance to the OPVs (8). Recent progress demonstrated simultaneous achievement of mechanical robustness and waterproof properties by embedding ultrathin OPVs in between elastomers (9), further expanding the application with textile compatibility.

To apply this technology ubiquitously, besides the requirement of a high PCE (10), improvement in thermal stability is of paramount importance to ensure a long lifetime under continuous operation even in harsh conditions (11, 12). Aging test of state-of-the-art rigid OPVs was mostly carried out with a glass-sealing encapsulation or in an inert atmosphere, which largely reveals the inherent stability of the active layers. OPVs having initial efficiencies of up to 10% (13), especially those with the fullerene acceptor [6,6]-phenyl-C_{71}-butyric acid methyl ester ($PC_{71}BM$), were reported to exhibit rapid degradation due to a general tendency of phase reorganization at high temperatures (14, 15). Strategies to suppress fullerene crystallization (16–18) including the use of cross-linking polymers, oligomeric fullerene derivatives, or other additives led to enhanced intrinsic stability of the OPVs. A representative system demonstrated that 80% of the initial PCE could be maintained after the devices were heated at 130 °C for 2 h in an inert atmosphere (19). The best-performing fullerene-free OPVs exhibited a T_{80} lifetime (defined as the lifetime when the efficiency of a device degrades by 20% from its initial PCE) (20) of over 250 h at 100 °C when encapsulated with

Significance

We have developed an ultraflexible organic photovoltaic (OPV) that achieves sufficient thermal stability of up to 120 °C and a high power conversion efficiency of 10% with a total thickness of 3 μm. By combining an inherently stable donor:acceptor blend as the active layer and ultrathin substrate and barriers with excellent thermal capability, we were able to overcome the trade-offs between efficiency, stability, and device thickness. The ultraflexible and thermally stable OPV can be easily integrated into textiles through the commercially available hot-melt process without causing performance degradation, thereby presenting great potential as a ubiquitous and wearable power source in daily life.

Author contributions: X.X., K.F., and T.S. designed research; X.X., K.F., S.P., H.K., H.J., N.W., S.Y., S.S., D.K., T.Y., and S.U. performed research; N.W., S.Y., S.S., and D.K. contributed new reagents/analytic tools; X.X., K.F., A.K., T.-Q.N., and T.S. analyzed data; and X.X., K.F., A.K., D.K., T.-Q.N., and T.S. wrote the paper.

The authors declare no conflict of interest.

This article is a PNAS Direct Submission.

[1]X.X. and K.F. contributed equally to this work.

[2]Present address: Department of Physics, Humboldt University of Berlin, 12489 Berlin, Germany.

[3]To whom correspondence may be addressed. Email: kenjiro.fukuda@riken.jp or takao.someya@riken.jp.

This article contains supporting information online at www.pnas.org/lookup/suppl/doi:10.1073/pnas.1801187115/-/DCSupplemental.

Published online April 16, 2018.

ENGINEERING

glass (21). Flexible OPVs have been explored employing reduced graphene oxide (22) or epoxy resin (23) to effectively enhance the stability under multiple aging conditions. The most stable system, poly (3-hexylthiophene) blended with fullerene acceptor as the active layer, was reported with 95% retained performance after 1,000 h under 85 °C and 85% relative humidity with an initial PCE of 2.7% (23).

Until now, however, there have been no documented OPVs that achieve sufficient thermal stability (above 100 °C), high efficiency (10%), and mechanical durability (micrometer-scale bending radius) simultaneously. Indeed, removal of the glass back support and encapsulation often leads to dramatically deteriorated cell performances. Due to the high gas permeability of a thin plastic substrate and passivation layer, especially when local temperature rises, the upkeep of device efficiency over a long run in ambient conditions require an intrinsically thermally stable active layer (24). Additionally, at elevated temperatures, conventional flexible substrates having relatively low glass-transition temperatures may result in irreversible performance degradation due to the induced mechanical strains during phase change (25).

Here we report a 3-μm-thick OPV system that exhibits an initial efficiency of up to 10% and demonstrates a remarkably enhanced thermal stability. The donor polymer, poly[4,8-bis(5-(2-ethylhexyl) thiophen-2-yl)benzo[1,2-b;4,5-b']dithiophene -2,6-diyl-alt-(4-octyl-3-fluorothieno[3,4-b]thiophene)-2-carboxylate-2–6-diyl] (PBDTTT-OFT, Fig. 1*C*), exhibits a high degree of face-on orientation when blended with $PC_{71}BM$, enabling a superior percolating network and maintaining a sturdy microstructure even when heated to 120 °C on an ultrathin substrate. Besides, the application of a thermally stable transparent polyimide substrate and Teflon/parylene double-barrier layers with minimal thicknesses guarantees a device long-term stability and high mechanical compliance simultaneously.

Device Structure and Performance

To demonstrate the applicability of thermally stable ultraflexible OPVs, we attached the 3-μm-thick OPVs onto textiles, as shown in Fig. 1*A*, using industrially available hot-melt adhesives (26) at 120 °C, which did not cause performance degradation. The detailed results will be discussed later. We designed the ultraflexible OPVs by embedding them between ultrathin plastics, i.e., a 1.3-μm-thick transparent polyimide substrate and 1.36-μm-thick Teflon/parylene double-barrier layers (Fig. 1*B*). The sequential stacks exhibited high uniformity, as revealed by the cross-section scanning electron microscope (SEM) image (*SI Appendix*, Fig. S1*A*). We adopted an inverted device structure to prevent direct contact between indium tin oxide (ITO) and poly(3,4-ethylenedioxythiophene): poly(styrenesulfonate) (PEDOT:PSS), thus avoiding proton etching of ITO and its subsequent degradation (27).

To achieve high efficiencies for the OPVs on the basis of ultrathin plastic substrate, transparent polyimide was chosen as the substrate film due to three important features, namely, high thermal stability, transparency, and surface flatness. The ultrathin transparent polyimide film having a glass transition temperature of 265 °C was stable during the subsequent high-temperature fabrication and worked without inducing mechanical strains (25). As indicated from the transmittance spectra, the transparency of the 1.3-μm-thick polyimide is comparable to that of glass in the visible spectrum. Besides, the transparent polyimide thin film exhibits a unique UV-cutoff property at a wavelength of around 360 nm (28) (*SI Appendix*, Fig. S1*B*), and could thus potentially suppress the UV-induced photochemical degradation (29). Additionally, the transparent polyimide thin film exhibits an ultrasmooth surface with a roughness of around 0.2 nm, and thus the top layers are as uniform as those cast on glass (*SI Appendix*, Fig. S2).

The ultraflexible OPVs demonstrate comparable PCEs as opposed to their rigid counterpart devices (Table 1). Statistics from 20 ultraflexible cells with active areas of 0.04 cm^2 show an average open-circuit voltage (V_{OC}) of 0.79 ± 0.01 V, short-circuit current density (J_{SC}) and fill factor (FF) of 17.2 ± 0.3 mA cm^{-2} and 69 ± 1%, respectively, and a PCE of 9.4 ± 0.2% under one-sun illumination. The current density–voltage (*J-V*) characteristic shown in Fig. 1*D* reveals the highest efficiency of 10% with

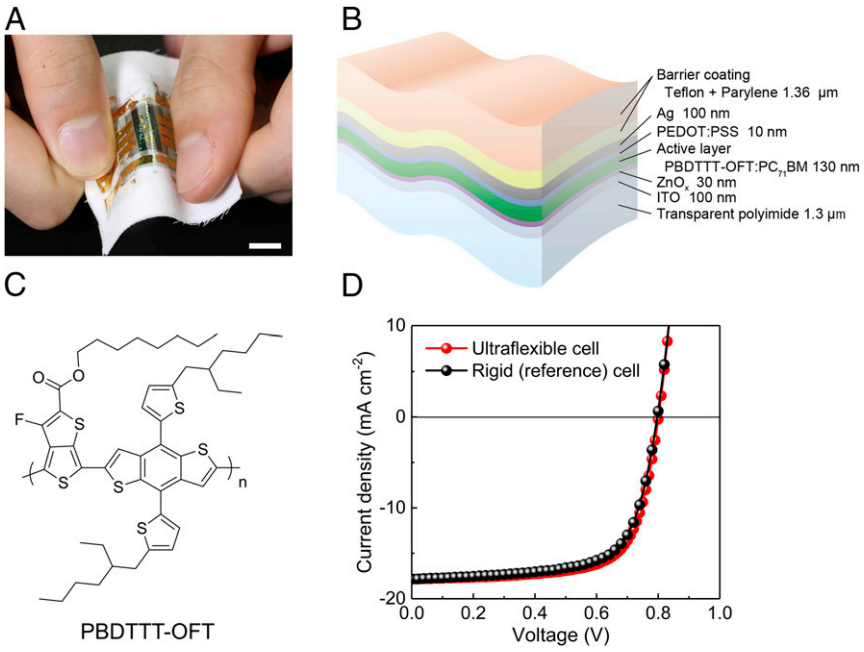

Fig. 1. Design and electrical performance of the ultraflexible OPV. (*A*) Photograph of 3-μm-thick OPVs adhered on textile after the instant hot-melt process. (Scale bar: 10 mm.) (*B*) A schematic showing the stacks in the ultrathin OPV design. (*C*) Chemical structure of the donor polymer, PBDTTT-OFT, developed in this study. (*D*) *J-V* scan of the best-performing 0.04 cm^2 OPVs under AM 1.5 irradiation. J_{SC} of 17.9 mA cm^{-2}, V_{OC} of 0.8 V, and FF of ∼0.70, and J_{SC} of 17.8 mA cm^{-2}, V_{OC} of 0.8 V, and FF of ∼0.68 corresponding to PCEs of 10.0 and 9.7% for the ultraflexible and rigid reference devices, respectively, were obtained.

Table 1. Photovoltaic parameters of the OPV single cells

Substrate	Active area, cm^2	J_{SC}, mA cm^{-2}	V_{OC}, V	FF, %	PCE, %
Glass	0.04	17.2 ± 0.3	0.79 ± 0.01	0.68 ± 0.01	9.2 ± 0.3 (9.7)
Transparent Polyimide	0.04	17.2 ± 0.3	0.79 ± 0.01	0.69 ± 0.01	9.4 ± 0.3 (10.0)
	0.16	17.1 ± 0.3	0.79 ± 0.01	0.67 ± 0.01	9.0 ± 0.2 (9.3)
	1.00	16.5 ± 0.5	0.79 ± 0.01	0.63 ± 0.01	8.2 ± 0.3 (8.8)

The statistics were calculated from 20 devices for each case. In the parentheses are maximum values from the best-performing devices.

excellent diode characteristics (*SI Appendix*, Fig. S3*A*) and negligible hysteresis (*SI Appendix*, Fig. S3*B*). The performances of the devices on transparent polyimide were slightly better than those of the devices on glass (*SI Appendix*, Fig. S3*C*). This is attributed to a higher shunt resistance and thus an enhanced FF (*SI Appendix*, Fig. S3*D*), indicating a highly continuous and flat transparent polyimide surface with fewer defects or microscopic pinholes (27, 30) that could induce inhomogeneity in the deposited layers on top.

Starting from well-known copolymers combining benzodithiophene (BDT) and thienothiophene (TT) moieties, which have narrow bandgaps and have been widely applied in OPVs with PCEs exceeding 10% (31), we designed a BDT-TT–type donor polymer, PBDTTT-OFT, with a linear alkyl side chain attached on the ester group of the fluorine-substituted TT unit. With a more stabilized as-cast packing and transport property compared with that of the branched counterpart polymer, poly[4,8-bis(5-(2-ethylhexyl)thiophen-2-yl)benzo[1,2-b;4,5-b']dithiophene-2,6-diyl- alt-(4-(2-ethylhexyl)-3-fluorothieno[3,4-b]thiophene)-2-carboxylate-2–6-diyl] (PBDTTT-EFT) (32, 33) (*SI Appendix*, Fig. S4*A*), both enhanced PCE and improved thermal stability can be expected (34). PBDTTT-OFT retains the coplanarity of the main chain and has a similar optical bandgap (E_g^{opt}) of 1.57 eV with an absorption onset at 790 nm (Fig. 2*A*) and a highest-occupied molecular orbital of 4.95 eV (*SI Appendix*, Fig. S4*B*). The PBDTTT-OFT blend film shows a slightly higher absorption coefficient ranging from 630 to 800 nm (Fig. 2*B*) than that of the PBDTTT-EFT:$PC_{71}BM$ blend.

Grazing-incidence wide-angle X-ray scattering (GIWAXS) measurement (Fig. 2*C*) reveals a predominant face-on packing of the pristine PBDTTT-OFT, showing well-defined π-π and lamellar peaks at $q_z \sim 1.65$ Å^{-1} (aromatic stacking spacing $d_1 = 3.80$ Å) and $q_y \sim 0.24$ Å^{-1} (lamellar stacking spacing $d_2 = 26.0$ Å). After blending with $PC_{71}BM$ (1:1.2 ratio), the sharp face-on packing peaks with high intensities were observed together with a broad reflection halo centered at $q \sim 1.37$ Å^{-1} (d spacing = 4.59 Å), which indicate a random orientation and short-range ordering of $PC_{71}BM$ aggregates. Compared with the PBDTTT-EFT:$PC_{71}BM$ film, which showed a ring-like lamellar peak, a weak and broad π-π peak in the out-of-plane direction at $q_z \sim 1.60$ Å^{-1} ($d_1 = 3.93$ Å) (35), the stronger reflections of PBDTTT-OFT imply a higher degree of crystallinity with face-on orientation. These consequently result in enhanced charge transport and improved PCE (*SI Appendix*, Fig. S4*C*). The optimal blend microstructure was further evidenced by a confined bimolecular recombination (*SI Appendix*, Fig. S4*D*).

Thermal Stability and Lifetime

The 3-μm-thick ultraflexible OPVs based on the PBDTTT-OFT:$PC_{71}BM$ blend exhibited superior high-temperature durability than the well-known PBDTTT-EFT:$PC_{71}BM$ blend having the same device structure did. After being heated in ambient air from 20 to 130 °C for 5 min under each step, the PBDTTT-EFT:$PC_{71}BM$ OPVs showed continuous performance deterioration, while the PCEs of the PBDTTT-OFT:$PC_{71}BM$ OPVs remained unchanged even when the temperature was raised to 100 °C (Fig. 3*A*). The ultraflexible PBDTTT-OFT:$PC_{71}BM$ OPVs could endure thermal stress at 100 °C for 4 h without any change in efficiency (*SI Appendix*, Fig. S5*A*). We observed a slight PCE deterioration by 7.4 and 13.8% of the initial efficiency when the PBDTTT-OFT:$PC_{71}BM$ cells were kept in air at 120 and 130 °C, respectively. On the other hand, the PCEs of the PBDTTT-EFT:$PC_{71}BM$ OPVs severely degraded by 37.6% at 130 °C with decreased J_{SC} and FF (*SI Appendix*, Fig. S5 *B* and *C*), which is mainly correlated with phase reorganization (36).

To gain insights into the intrinsic stability of the bulk heterojunctions, we performed comparative study of the two blends by subjecting the OPVs to thermal stress over a relatively long time inside a glove box. After heating at 130 °C for 4 h in N_2 atmosphere, a drastic decrease in the photocurrent from 92 to 39 pA by 58% was observed in the PBDTTT-EFT:$PC_{71}BM$ film by mapping with photoconductive atomic force microscopy (AFM) (37) (Fig. 3*C*), which revealed undesired transport degradation that led to PCE loss. This is consistent with the bicontinuous topography change in dimensions (*SI Appendix*, Fig. S6), which indicates phase reorganization under thermal stress. In comparison, the microstructure of the PBDTTT-OFT:$PC_{71}BM$ film shows robustness under the same annealing condition, maintaining a photocurrent of 142 pA, which is responsible for the retention of high PCE. This optimal as-cast microstructure yields a high efficiency and excellent thermal stability simultaneously (13).

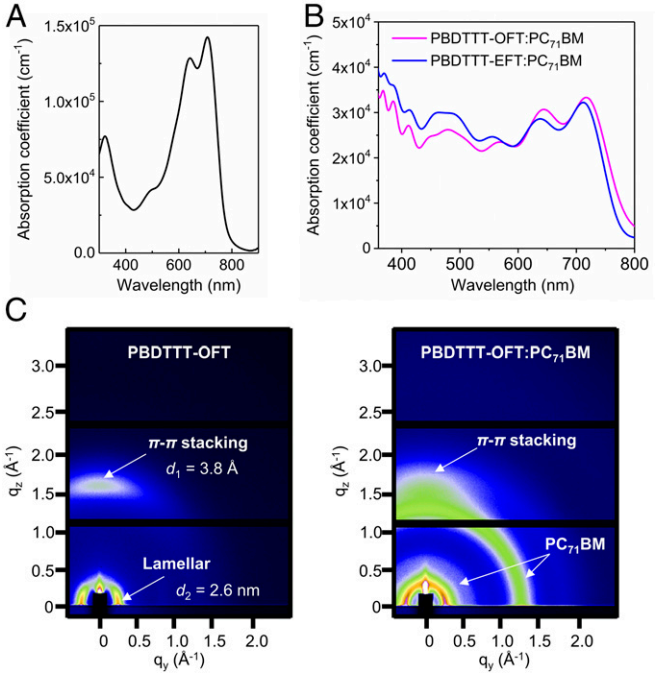

Fig. 2. Thin-film characterization. (*A*) UV-vis absorption spectrum of the pristine PBDTTT-OFT thin film. (*B*) UV-vis absorption spectrum of the PBDTTT-OFT:$PC_{71}BM$ and PBDTTT-EFT:$PC_{71}BM$ blend films. (*C*) Two-dimensional GIWAXS images of the pristine PBDTTT-OFT film and the PBDTTT-OFT:$PC_{71}BM$ blend film.

ENGINEERING

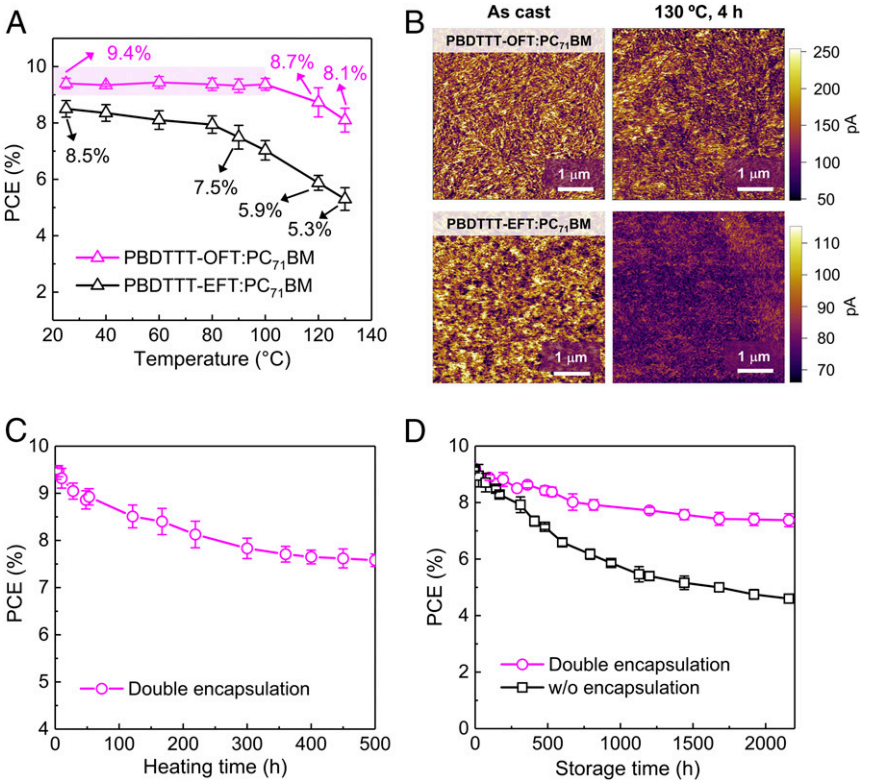

Fig. 3. Thermal stability and lifetime of the ultraflexible OPV. (*A*) Short-time thermal stability comparison between OPVs with PBDTTT-OFT:$PC_{71}BM$ and PBDTTT-EFT:$PC_{71}BM$ blends, with the same device structure and heat-treated in ambient air. (*B*) AFM photocurrent images collected under a white-light source with a power of 30 W cm^{-2} of PBDTTT-OFT:$PC_{71}BM$ (*Top*) and PBDTTT-EFT:$PC_{71}BM$ (*Bottom*) blends before (*Left*) and after (*Right*) thermal treatment at 130 °C for 4 h in a glove box. The photoactive films were deposited on transparent polyimide/ITO/ZnO substrates with glass support. The photocurrent images were collected using a chromium/platinum AFM probe with a bias applied to the substrate. (*C*) Aging test of the PBDTTT-OFT:$PC_{71}BM$-based 3-μm-thick ultraflexible OPVs under thermal stress at 85 °C in air. (*D*) Storage lifetime comparison between the ultraflexible cells encapsulated with 1.36-μm Teflon/parylene double barriers (magenta hollows) and the glass-supported rigid devices without encapsulation (dark-gray squares).

As shown in the photoconductive AFM results (Fig. 3*B*), the PBDTTT-OFT:$PC_{71}BM$ blend film is more thermally robust than the PBDTTT-EFT:$PC_{71}BM$ film. The improved thermal stability can be ascribed to the favorable packing of molecules due to the difference in the side chains of the two compounds. The side chain of PBDTTT-EFT is a branched ethylhexyl group, whereas the side chain of PBDTTT-OFT is a linear octyl. In general, linear alkyl chains lead to films with higher crystallinity and reduce the diffusion rates of water and oxygen through the film, as compared with amorphous/disordered films, which improves the thermal stability of PBDTTT-OFT:$PC_{71}BM$ films. Indeed, the crystallinity of PBDTTT-OFT:$PC_{71}BM$ is better than that of PBDTTT-EFT:$PC_{71}BM$, as observed from the GIWAXS results (Fig. 2*C* and *SI Appendix*, Fig. S6*C*). All of these allude to the fact that compound PBDTTT-OFT is indeed responsible for an improved thermal stability.

Next, we performed an aging test following the international summit on OPV stability (ISOS) protocol (38). The ultraflexible OPVs with 1.36-μm-thick Teflon/parylene double-barrier layers were kept at 85 °C in air under controlled humidity of 30% according to ISOS-D-2. We observed an averaged T_{80} of over 500 h under continuous thermal stress (Fig. 3*C*).

The plastic barriers significantly prolong the device storage lifetime to >2,000 h at room temperature (ISOS-D-1 protocol) compared with the nonencapsulated devices (around 400 h, Fig. 3*D*) and parylene single-layer encapsulated devices (*SI Appendix*, Fig. S7). Since there is a trade-off between barrier thickness and device lifetime (9), the double-layer barriers demonstrated here offer a solution to maintaining the ultrathinness simultaneously with strong barrier property, and thus, excellent environmental stability of the devices.

Scalability and Mechanical Compliance

The scalability of the ultraflexible OPVs interpreted by the average photovoltaic parameters with different working areas is summarized in Table 1. The fabrication processes involve sequential depositions of the stacks on transparent polyimide-coated supporting glass plates, followed by a delamination process that causes no obvious deterioration of the electrical performance (*SI Appendix*, Fig. S8 *A–C*). With the aperture area increased to 0.16 and 1.0 cm^2, the ultraflexible devices still retain a V_{OC} of 0.79 V and exhibit maximum PCEs of 9.3 and 8.8%, respectively (Table 1 and *SI Appendix*, Fig. S8*D*). The short-circuit currents from the *J-V* measurements are in good agreement with the calculated J_{SC} obtained by integrating the external quantum efficiency (EQE, *SI Appendix*, Fig. S8*E*).

We further fabricated multiple 3-μm-thick solar modules with a substrate size of 5 × 5 cm^2. The module illustrated in Fig. 4 *A* and *B* has a total working area of 4.4 cm^2, a per-area mass of 5.4 g m^{-2}, an overall PCE of 8.2%, and a power-per-weight of up to 16.7 g W^{-1}, generating a power output of around 36 mW under one-sun illumination (Fig. 4*C*). A decorative sunflower-shaped module, as depicted in *SI Appendix*, Fig. S8 *F* and *G*, generates 20 mW power under one-sun illumination. The excellent scalability with high efficiency is due to the great uniformity of the as-cast PBDTTT-OFT:$PC_{71}BM$ blend. A complete intermixing between the donor polymer and $PC_{71}BM$, which is insensitive to deposition temperatures, offers viability in practical

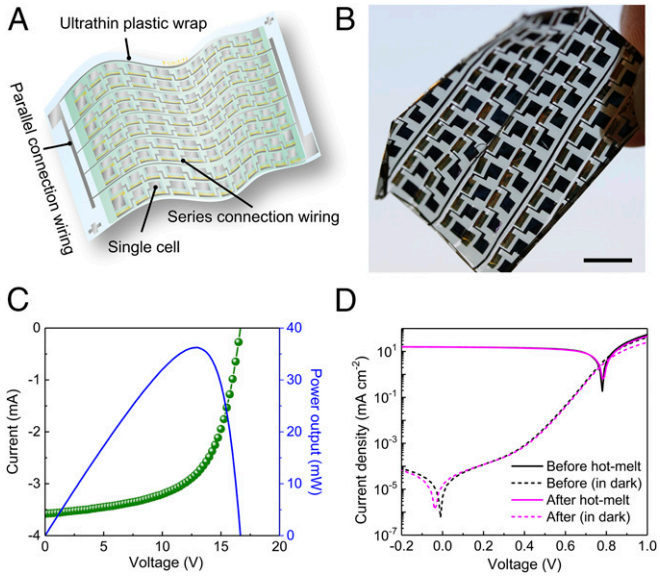

Fig. 4. Solar modules and textile compatible OPVs. (*A*) Schematic of a 5 × 5-cm^2 ultraflexible solar module with five parallel-connected arrays, each containing 22 single cells in series connection. (*B*) Photo image of the solar module illustrated in *A*. (Scale bar: 1 cm.) (*C*) *J-V* scan and power output of the solar module illustrated in *A*. (*D*) Diode characteristics of an ultraflexible OPV before and after the hot-melt process, showing no electrical degradation.

roll-to-roll production of large-area flexible modules under room temperature.

The modules endure repeated rolling, folding, or crumpling without obvious cracks or performance deterioration (*SI Appendix*, Fig. S9). This high level of compliance suggests that the devices can be stretchable using the buckling phenomenon. To demonstrate the stretchability of the OPV cells, we transferred the 3-μm-thick OPVs on a prestretched acrylic elastomer. Releasing the elastomer applies compression strain to the closely attached ultrathin OPVs, and the resulting sinusoidal waves, as revealed by the SEM image, showed a bending radius of ∼10 μm when the devices were compressed by 50%. We were able to perform a cyclic compression/stretching test with a maximum strain of 66.7% applied for 100 cycles, and observed only 12% degradation in the initial efficiency. This further suggests good mechanical property of our high-performance OPVs.

Hot-Melt Process

Attaching ultraflexible OPVs onto textiles by an instant and low-cost process can significantly expand their potential applications. Indeed, we anticipate that flexible OPVs possessing extraordinary thermal durability would allow a facile bonding onto textiles through the hot-melt adhesive technology (39). Our ultraflexible OPVs with good stability at temperature over 100 °C makes this design possible. For a prototype demonstration of wearable OPVs, we applied an instant hot-melt process at 120 °C and 15 kPa for 30 s using a polyurethane melt film, and observed no performance degradation after this process (Fig. 4*D* and *SI Appendix*, Fig. S10). Because of the minimized thickness and a bending radius of 10 μm, our OPVs are fully compatible with textiles without any incongruity and do not interfere with the movement of the clothes.

Conclusion

We demonstrate a design of OPVs that have remarkably enhanced thermal stability and exhibit a high PCE among all of the flexible OPVs featuring extreme mechanical compliance. This high performance under thermal stress is mainly attributed to an optimal and robust microstructure of the PBDTTT polymer: $PC_{71}BM$ blend. The ultrathin plastic substrate and barrier coatings with good thermal capability and low gas permeability further allow the operation of the cells and their storage in air or under harsh conditions over a long period. In combination with the mature hot-melt process in the apparel industry, our thermally stable and ultraflexible OPVs can greatly expand the possibilities of textile-compatible electronics.

Methods

Material Synthesis and Characterization. The synthetic procedures for PBDTTT-OFT are detailed in *SI Appendix*. All of the results are obtained from PBDTTT-OFT with molecular mass (M_n) of around 40 kDa and a polydispersity below 2.2.

Thin-Film Characterization. Thin-film thicknesses were determined with a surface profiler (DEKTAK 6M; Bruker). UV-vis absorption spectra were recorded on a JASCO V-670 spectrophotometer. Two-dimensional GIWAXS measurements were conducted at beamline BL46XU of SPring-8. The irradiation wavelength was λ = 0.10 nm (energy: 12.4 keV) and the incident angle was fixed at 0.12°. The GIWAXS patterns were recorded by a Pilatus 300K 2D image detector with a camera length of 170.3 mm. The irradiation time was fixed at 1 s for all of the samples. Polymer and bulk heterojunction samples were prepared on Si substrates by spin-coating. AFM images were obtained with a Shimadzu SPM-9700HT scanning probe microscope in the tapping mode. Photoconductive AFM measurements were done with an Asylum Research MFP-3D microscope sitting atop an inverted optical microscopy (IX71; Olympus). The photoactive films were deposited on transparent polyimide/ITO/zinc oxide (ZnO) substrates with glass support and scanned under inert atmosphere. A white-light source with a power of 30 W cm^{-2} was used to generate photocurrent which was recorded by an internal preamplifier (Asylum Research ORCA head model). Chromium/platinum-coated silicon probes with a spring constant of 0.2 N m^{-1} and resonant frequency of 13 kHz (Budget Sensors) were used. The light was focused on the sample through an inverted optical microscope (Olympus), and the tip was positioned at the center of the light spot, which was ∼160 μm in diameter.

Device Fabrication and Characterization. The OPV devices were manufactured on 1.3-μm-thick transparent polyimide and then packaged with 1.36-μm barrier coatings. Finally, they were detached into a freestanding state with a total thickness of 3 μm. To fabricate the transparent polyimide substrate, a precursor (ECRIOS, Mitsui Chemicals, Inc.) was first spin-coated on a glass plate with the surface pretreated by a fluorinated polymer layer (Novec 2702; 3M Company), followed by an imidization reaction at 270 °C for 2 h in N_2 atmosphere. After the curing treatment, the ultrathin transparent polyimide substrate forms a highly cross-linked structure, which is directly responsible for mechanical and temperature strength. Encapsulation of the finishing device was realized with ultrathin plastic barriers, including a 360-nm-thick Teflon (AF 1600; Dupont) layer spin-coated and cured at 100 °C for 0.5 h, together with a 1-μm-thick parylene (diX-SR; Daisan Kasei Co., Ltd.) layer formed by chemical vapor deposition. The main effective stacks adopted an inverted OPV structure: ITO/ZnO/active layer/PEDOT:PSS/Ag. The 100-nm-thick ITO layer was formed as a transparent electrode by sputtering. The 30-nm ZnO layer, i.e., the electron transporting layer (hole-blocking layer), was deposited by a sol–gel method. The ZnO precursor solution was prepared by dissolving zinc acetate dehydrate (0.5 g) and ethanolamine (0.14 mL) in 5 mL 2-methoxyethanol, and then spin-coated (MS-B100 Spin-Coater, Mikasa; 5,000 rpm for 30 s) on top of ITO, followed by baking in air at 180 °C for 30 min. The active layer, PBDTTT-OFT:$PC_{71}BM$ (about 110 nm), was deposited in a glove box by spin-coating a Chlorobenzene solution (with 2% 1,8-Diiodooctane additive) containing PBDTTT-OFT and $PC_{71}BM$ with a weight ratio of 1:1.2 (sonicate for 0.5 h for complete dissolution) at 600 rpm for 20 s (MS-B100 Spin-Coater, Mikasa). The thin film was then dried in vacuum for 0.5 h. The counterpart active layer of PBDTTT-EFT:$PC_{71}BM$ (1:1.5, wt/wt) was spin-coated at 1,500 rpm for 60 s (MS-B100 Spin-Coater, Mikasa) from its solution in chlorobenzene/DIO (97:3 vol/vol, stir for 24 h for a complete dissolving), and dried overnight. A thin layer of PEDOT:PSS with a thickness of around 10 nm, i.e., hole transporting layer (electron-blocking layer) was spin-coated (MS-B100 Spin-Coater, Mikasa; 2,000 rpm for 30 s) from a 2-propanol solution (15% in volume) and annealed at 80 °C on a hot plate for 5 min inside the glove box. Finally, Ag (100 nm) anode was deposited through a shadow mask in a vacuum evaporator. Large-area modules with the same device architecture were fabricated using designed masks for patterning. The OPV single cells and modules were characterized under simulated solar illumination (AM 1.5 global spectrum, 100 mW cm^{-2} calibrated with a standard

silicon reference diode). The *J-V* characteristics were recorded using a Keithley 2400 source meter at a rate of 0.17 V s^{-1} in ambient atmosphere. Additional gold wirings (100 nm Au deposited on 12.5-μm-thick polyimide films) were used to improve the connection between the freestanding devices and the source meter. EQE was measured with monochromatic light (SM-250F; Bunkoh-Keiki).

Stability Test. To examine the thermal stability following the ISOS-D-2 protocol, the devices were incubated in an oven (SH-242 Bench-top Type Temperature & Humidity Chamber; Espec) at a controlled temperature of 85 °C and humidity of 30% RH. The shelf life was measured following the ISOS-D-1 protocol, i.e., devices being stored in ambient conditions (in a light-shielded desiccator at a controlled temperature of 25 °C and humidity of 30%), with periodic testing under AM 1.5 illumination in ambient atmosphere. To perform the compression/stretch cyclic test, freestanding OPVs were first laminated on a prestretched acrylic elastomer (3M VHB Y-4905J), whose two ends were fixed on a mechanical stage. The elastomer was prestretched by 200% at the initial state and then released in steps with a maximum compression strain of 66.7% applied to the OPVs. The actual working area of the device in the compressed state was calculated from the optical photographs under each compressive strain, and the device PCE was calibrated by considering the change in the actual projection area.

ACKNOWLEDGMENTS. We thank Dr. K. Tajima, Dr. K. Nakano, and Dr. D. Miyajima of Center for Emergent Matter Science, RIKEN (Japan), Dr. I. Amimori, O. Sawanobori, and A. Hitomi in Xenoma, Inc. (Japan) for helpful discussions and technical support. This work was supported by Japan Science and Technology Agency (JST), Exploratory Research for Advanced Technology Grant JPMJER1105 and JST Precursory Research for Embryonic Science and Technology Grant JPMJPR1428. A.K. and T.-Q.N. acknowledge the support from the Department of the Navy, Office of Naval Research (Award N00014-14-1-0580).

1. Zhao J, et al. (2016) Efficient organic solar cells processed from hydrocarbon solvents. *Nat Energy* 1:15027–15040.
2. Dai S, et al. (2017) Fused nonacyclic electron acceptors for efficient polymer solar cells. *J Am Chem Soc* 139:1336–1343.
3. Li M, et al. (2017) Solution-processed organic tandem solar cells with power conversion efficiencies >12%. *Nat Photonics* 11:85–90.
4. Zhao F, et al. (2017) Single-junction binary-blend nonfullerene polymer solar cells with 12.1% efficiency. *Adv Mater* 29:1700144.
5. Zhao W, et al. (2017) Molecular optimization enables over 13% efficiency in organic solar cells. *J Am Chem Soc* 139:7148–7151.
6. Lim JW, et al. (2012) Mechanical integrity of flexible Ag nanowire network electrodes coated on colorless PI substrates for flexible organic solar cells. *Sol Energy Mater Sol Cells* 105:69–76.
7. Yao K, et al. (2015) Enhanced light-harvesting by integrating synergetic microcavity and plasmonic effects for high-performance ITO-free flexible polymer solar cells. *Adv Funct Mater* 25:567–574.
8. Kaltenbrunner M, et al. (2012) Ultrathin and lightweight organic solar cells with high flexibility. *Nat Commun* 3:770.
9. Jinno H, et al. (2017) Stretchable and waterproof elastomer-coated organic photovoltaics for washable electronic textile applications. *Nat Energy* 2:780–785.
10. Lucera L, et al. (2016) Highly efficient, large area, roll coated flexible and rigid OPV modules with geometric fill factors up to 98.5% processed with commercially available materials. *Energy Environ Sci* 9:89–94.
11. Krebs FC (2012) *Stability and Degradation of Organic and Polymer Solar Cells* (John Wiley & Sons, West Sussex, UK).
12. Cheng P, Zhan X (2016) Stability of organic solar cells: Challenges and strategies. *Chem Soc Rev* 45:2544–2582.
13. Baran D, et al. (2017) Reducing the efficiency-stability-cost gap of organic photovoltaics with highly efficient and stable small molecule acceptor ternary solar cells. *Nat Mater* 16:363–369.
14. Jørgensen M, Norrman K, Krebs FC (2008) Stability/degradation of polymer solar cells. *Sol Energy Mater Sol Cells* 92:686–714.
15. Hsieh Y-J, et al. (2017) Insights into the morphological instability of bulk heterojunction PTB7-Th/PCBM solar cells upon high-temperature aging. *ACS Appl Mater Interfaces* 9:14808–14816.
16. Rumer JW, McCulloch I (2015) Organic photovoltaics: Crosslinking for optimal morphology and stability. *Mater Today* 18:425–435.
17. Ramanitra HH, et al. (2016) Increased thermal stabilization of polymer photovoltaic cells with oligomeric PCBM. *J Mater Chem C* 4:8121–8129.
18. Derue L, et al. (2014) Thermal stabilisation of polymer-fullerene bulk heterojunction morphology for efficient photovoltaic solar cells. *Adv Mater* 26:5831–5838.
19. Cheng P, et al. (2016) Molecular lock: A versatile key to enhance efficiency and stability of organic solar cells. *Adv Mater* 28:5822–5829.
20. Gevorgyan SA, et al. (2016) Baselines for lifetime of organic solar cells. *Adv Energy Mater* 6:1600910.
21. Zhao W, et al. (2016) Fullerene-free polymer solar cells with over 11% efficiency and excellent thermal stability. *Adv Mater* 28:4734–4739.
22. Kim T, et al. (2012) Facile preparation of reduced grapheme oxide-based gas barrier films for organic photovoltaic devices. *Energy Environ Sci* 7:3403–3411.
23. Sapkota SB, Spies A, Zimmermann B, Dürr I, Würfel U (2014) Promising long-term stability of encapsulated ITO-free bulk-heterojunction organic solar cells under different aging conditions. *Sol Energy Mater Sol Cells* 130:144–150.
24. Giannouli M, et al. (2015) Methods for improving the lifetime performance of organic photovoltaics with low-costing encapsulation. *Chemphyschem* 16:1134–1154.
25. Lin Q, et al. (2016) High performance thin film solar cells on plastic substrates with nanostructure-enhanced flexibility. *Nano Energy* 22:539–547.
26. de Avila Bockorny G, et al. (2016) Modifying a thermoplastic polyurethane for improving the bonding performance in an adhesive technical process. *App Adhes Sci* 4:4.
27. Wang K, Liu C, Meng T, Yi C, Gong X (2016) Inverted organic photovoltaic cells. *Chem Soc Rev* 45:2937–2975.
28. Abe A, et al. (2011) Theoretical and experimental studies on the mechanism of coloration of polyimides. *Chemphyschem* 12:1367–1377.
29. Jeong J, et al. (2015) Significant stability enhancement in high-efficiency polymer: Fullerene bulk heterojunction solar cells by blocking ultraviolet photons from solar light. *Adv Sci (Weinh)* 3:1500269.
30. Zhang H, et al. (2016) Pinhole-free and surface-nanostructured NiOx film by room-temperature solution process for high-performance flexible perovskite solar cells with good stability and reproducibility. *ACS Nano* 10:1503–1511.
31. Zhang S, Ye L, Hou J (2016) Breaking the 10% efficiency barrier in organic photovoltaics: Morphology and device optimization of well-known PBDTTT polymers. *Adv Energy Mater* 6:1502529.
32. Liao S-H, Jhuo H-J, Cheng Y-S, Chen S-A (2013) Fullerene derivative-doped zinc oxide nanofilm as the cathode of inverted polymer solar cells with low-bandgap polymer (PTB7-Th) for high performance. *Adv Mater* 25:4766–4771.
33. He Z, et al. (2015) Single-junction polymer solar cells with high efficiency and photovoltage. *Nat Photonics* 9:174–179.
34. Liang Y, et al. (2009) Highly efficient solar cell polymers developed via fine-tuning of structural and electronic properties. *J Am Chem Soc* 131:7792–7799.
35. Mai J, et al. (2017) High efficiency ternary organic solar cell with morphology- compatible polymers. *J Mater Chem A* 5:11739–11745.
36. Ray B, Alam MA (2011) A compact physical model for morphology induced intrinsic degradation of organic bulk heterojunction solar cell. *Appl Phys Lett* 99:033303.
37. Dang X-D, et al. (2010) Nanostructure and optoelectronic characterization of small molecule bulk heterojunction solar cells by photoconductive atomic force microscopy. *Adv Funct Mater* 20:3314–3321.
38. Reese MO, et al. (2011) Consensus stability testing protocols for organic photovoltaic materials and devices. *Sol Energy Mater Sol Cells* 95:1253–1267.
39. Yorkgitis EM (2001) *Adhesive Compounds-Encyclopedia of Polymer Science and Technology* (John Wiley & Sons, New York).